

---

## Developing a new wind dataset by blending satellite data and WRF model wind predictions

Salvação Nadia <sup>1</sup>, Bentamy Abderrahim <sup>2</sup>, Guedes Soares C. <sup>1,\*</sup>

<sup>1</sup> Centre for Marine Technology and Ocean Engineering (CENTEC), Instituto Superior Técnico, Universidade de Lisboa, Av. Rovisco Pais, 1049-001, Lisboa, Portugal

<sup>2</sup> Laboratoire Spatial et Interfaces Air-Mer (IFREMER), Centre Bretagne - ZI de la Pointe du Diable, CS 10070-29280, Plouzané, France

\* Corresponding author : Soares C. Guedes, email address :  
[c.guedes.soares@centec.tecnico.ulisboa.pt](mailto:c.guedes.soares@centec.tecnico.ulisboa.pt)

---

### Abstract :

This paper presents an approach to improve wind datasets developed using the regional atmospheric model Weather Research Forecasting by combining its predictions with remotely sensed wind observations in enhanced wind speed analyses that leads to blended winds. In this study, satellite data derived from scatterometers, radiometers, and synthetic aperture radar are used. The spatial and temporal features of each wind product are thoroughly analysed. For the probabilistic evaluation of their skill, comprehensive comparisons with available buoy data are carried out. The statistical analysis shows that the combined use of satellite and numerical weather prediction model data improves the agreement with buoy measurements, demonstrating the added value of using the blended product. As an application of the method, new improved satellite wind speeds are presented in the form of a wind energy assessment along the Iberian coastal area. From inspection of the provided wind power maps, northern and central regions emerge as the most promising areas for wind harnessing offshore despite some seasonal variations. Finally, potential wind farm sites are provided, along with insights into multi-year wind speed distribution. The results show how the new dataset can be used for the selection of promising areas for wind

**Keywords** : WRF, Satellite wind, blended data, wind energy

# 32 **1 Introduction**

33

34 Improving the skill of wind speed predictions and understanding its regional patterns, brings  
35 numerous economic and technical advantages [1-2], in particular for the wind energy industry, which

36 is expanding offshore at a fast pace [3-6]. In the present day, the spatial distribution of wind resources  
37 is still a major element for the siting of offshore wind parks [7-10]. Having adequate climate services  
38 and adopting the existing ones persists as a big challenge for the wind energy sector [11].

39 Several wind datasets are publicly available, allowing for a quick evaluation of the regions with  
40 greater wind exploitation potential. Examples are reanalysis datasets such as Era-interim [12] and  
41 Era5 [13] or MERRA-2 [14]. However, these lack the necessary spatial resolution and are not capable  
42 of addressing each site's unique local climatic characteristics which highly affects wind power peaks  
43 and ramps predictions [15]. The Global Wind Atlas and the New European Wind Atlas are also widely  
44 used tools for wind energy assessment and have even been used in combination with reanalysis data  
45 for bias correction, but research found some versions of this product to be inefficient in improving  
46 simulation quality [16].

47 Similarly, numerical weather prediction (NWP) models are also one of the most widely used tools for  
48 wind assessment [17-18]. Various studies have further pointed out the WRF model as an effective  
49 wind assessment tool [19-20]. WRF has been proved to be a useful model to assess wind resources  
50 in various countries such as Oman [21], Northern Europe [22], Iceland [23], Portugal [24], and  
51 therefore it has been chosen to perform this study.

52 Although several resource assessment systems have been developed to provide accurate estimates of  
53 the available wind power across different regions, the current deterministic NWP models regardless  
54 of their demonstrated skill, have several limitations as they only represent a single wind trajectory for  
55 each site and consequently one future scenario of the energetic conditions and high dependence upon  
56 the initial conditions. Ensembles of simulations have been proved to improve this situation [25-27].  
57 Despite its indisputable capabilities, NWP models still have a large margin for improvement. Novel  
58 improved methods can significantly reduce the risk and uncertainty for both the planning and  
59 maintenance stages of wind parks. A new design for wind and wind power forecasting designed by  
60 combining the results of WRF with fuzzy clustering, association rule and optimization methodologies  
61 can be effective in reducing the uncertainty of wind farm forecasting [28]. In this study, the strengths  
62 that NWP offer are combined with satellite data to improve their skill.

63 Therefore, combining NWP models with other sources of information can diminish the uncertainty  
64 of wind speed forecasts, especially if they have been tuned to give the most accurate conditions for a  
65 specific site. To take advantage of the strengths of multiple products, the joint use of distinct wind  
66 data sources tailored to the needs of each application has been widely employed over the last years  
67 [29-31]. A study [32] reconstructed one year of wind data from multiple satellite information and the  
68 WRF model to analyse the offshore wind resources over the South China Sea. The developed  
69 methodology provides a valuable tool for a well-informed site selection. This is of major interest for  
70 offshore areas where few in situ observations are available. Despite the demonstrated capabilities of

71 NWP models, there are numerous advantages of using other sources of information. For instance,  
72 remote sensing data is capable of resolving fine-scale structures not fully captured by these models  
73 [33].

74 Satellite information has been recently used to assess the spatial variability of global ocean wind  
75 resources [34-35]. While satellite data contribute to spatial and temporal coverage, buoy data consists  
76 of a long and accurate time series of wind observations capable of describing the true wind conditions  
77 and providing information on the diurnal and seasonal/annual variability of the wind resource.

78 As concerns the Portuguese coastal zone, the study area considered in this work, the need for  
79 improved understanding of the wind patterns along the Iberian coastal zone drove several works that  
80 aimed at determining the most suitable areas for wind exploitation. Satellite data confirm that the  
81 Portuguese coastline has the potential to generate large amounts of electricity [36-37] showing that  
82 four main areas with homogeneous wind conditions can be devised on the Portuguese coast [35]. For  
83 example, a 10-year hindcast for the Iberian Peninsula coast demonstrated the WRF model's ability to  
84 express the local wind across the selected domain [24]. Also, for the Iberian Peninsula, another study  
85 [38] presents projections of future climate scenarios using a set of models that proved to successfully  
86 hindcast inland and offshore winds. The statistical properties of the data were analysed and it was  
87 shown that four main areas with homogeneous wind conditions could be devised on the Portuguese  
88 coast [39]. To address the challenges of the most commonly used wind resource assessment methods,  
89 this study aims to provide an accurate wind product capable of improving the existing data and  
90 provide accurate local resource estimation using two of the most accurate sources of wind data,  
91 numerical models and satellite data.

92 For this purpose, in this work, surface wind observations, retrieved from several satellite  
93 scatterometer and radiometer measurements, are combined with a 9-year (2004 – 2012) wind hindcast  
94 produced by the WRF model, resulting in new time series of blended wind estimates. The main  
95 strength of this method is that it uses the most suitable model configuration for the area of interest in  
96 combination with accurate satellite data that can correct the known deficiencies of NWP models such  
97 as wind magnitude bias. After validating the blended winds against a dataset of wind measurements  
98 obtained from a network of meteorological buoys, the temporal and spatial variability along the  
99 Iberian coast is examined in more detail.

100 The annual and seasonal variability as well as the mean extreme wind speed thresholds are also  
101 presented. The statistical characterization of wind power errors is performed. In this framework, the  
102 extreme wind speed in a given return period is used as a reference for survivability studies of the  
103 floating wind devices. The statistical percentile technique (90%, 95%, and 99%) and maxima over a  
104 specific period are some of the most commonly employed approaches to determine such a reference  
105 value [40]. To that end, the spatial distribution of the 99th percentile of the yearly wind speed is also

106 mapped. The final aim is to build a new dataset of winds to produce high-resolution wind maps that  
107 can be used as a site selection tool for offshore and coastal projects.

110 This paper is organized in the following manner: section 2 briefly discusses the WRF model, the  
111 satellite analyses, buoy data and its agreement with observations; section 3 provides information  
112 about the Iberian coast wind patterns, the seasonal and intra-annual variations and extreme  
113 distribution of the wind. A comprehensive analysis of renewable energy follows in section 4 along  
114 with energy maps able to describe the available resources. Finally, a brief discussion of the results is  
115 presented in section 5.

116

117

## 118 **2 Data**

### 119 **2.1 In-situ wind measurements**

120

121 The main source of surface wind used is from buoys located in the Atlantic Ocean along the  
122 North of Spain (South of Biscay Bay), western areas of Spain and Portugal, and Southwest of Spain  
123 (Table 1). Buoy data are provided by Puertos Del Estado (Spain), Xunta De Galicia (Spain), and  
124 Instituto Hidrográfico (Portugal). They are made available as Copernicus Marine Environment  
125 Monitoring Service (CMEMS ([marine.copernicus.eu](http://marine.copernicus.eu))) products. More specifically, buoy data are  
126 retrieved from the CMEMS platform “European Marine Observation and Data Network” (EMODnet)  
127 [41].

128 Most of the buoy data (>98%) are available in hourly estimates. In addition to wind speed and  
129 direction information, both provided at anemometer heights (3 m), buoy measurements of required  
130 atmospheric and oceanic parameters such as temperatures and relative humidity are also provided.  
131 The use of quality control flags, available with data, allow the consistent assessment of reliable wind  
132 speed time series. To avoid the use of inhomogeneous (erroneous) data, not detected through the  
133 standard quality control process, or to reject correct data, each buoy time series is investigated  
134 individually, and proper selected statistical criteria are determined and applied. More specifically, for  
135 each month of the study period and each buoy, monthly-averaged buoy wind estimates, and the  
136 associated standard deviations, are calculated from the available buoy wind measurements. Buoy data  
137 exceeding three standard deviations monthly values are investigated individually. Hourly buoy winds  
138 are converted to 10m neutral winds using COARE3.0 parameterizations [42].

139

140

141

Table 1: Buoy information including buoy WMO code, coordinates (latitude, longitude), period of data availability, mean 10m wind speed (Mean), standard deviation (STD), skewness (Skew), kurtosis (Kur), 5% (P<sub>05</sub>) and 95% (P<sub>95</sub>) quartiles.

WMO Code	Latitude	Longitude	Period	Mean (m/s)	STD (m/s)	Skew	Kur	P <sub>05</sub> (m/s)	P <sub>95</sub> (m/s)
6200191	41.1500°N	9.5800°W	2010-2019	7.61	3.87	0.37	2.87	1.78	14.25
6200192	39.5100°N	9.6400°W	2009-2019	7.45	3.70	0.60	3.69	2.00	13.80
6200199	39.5600°N	9.2100°W	2010 - 2019	6.17	3.38	0.60	2.96	1.34	12.29
6201031	41.9011°N	8.8993°W	2010 - 2019	7.30	3.62	0.42	3.15	1.83	13.49
6201038	42.6295°N	8.7804°W	2007 - 2019	5.39	3.05	0.49	2.89	0.94	10.73
6201040	42.1719°N	8.9063°W	2008 - 2019	5.97	3.81	1.17	5.87	1.08	12.71
6201062	42.5500°N	8.9475°W	2011 - 2019	6.92	4.76	1.47	6.19	1.09	14.75
62025	43.7419°N	6.1679°W	1997 - 2019	6.03	3.64	0.67	3.07	1.07	12.71
62082	44.0896°N	7.6428°W	1996 - 2019	7.80	4.02	0.56	3.73	1.67	14.49
62083	43.4963°N	9.2134°W	1998 - 2019	7.81	4.16	0.29	2.53	1.39	14.96
62084	42.1225°N	9.4142°W	1998 - 2019	7.11	3.93	0.30	2.41	1.31	13.78
62085	36.4953°N	6.9650°W	1996 - 2019	6.30	3.33	0.55	3.07	1.43	12.24

142

143

144

145

146

147

148

149

150

151

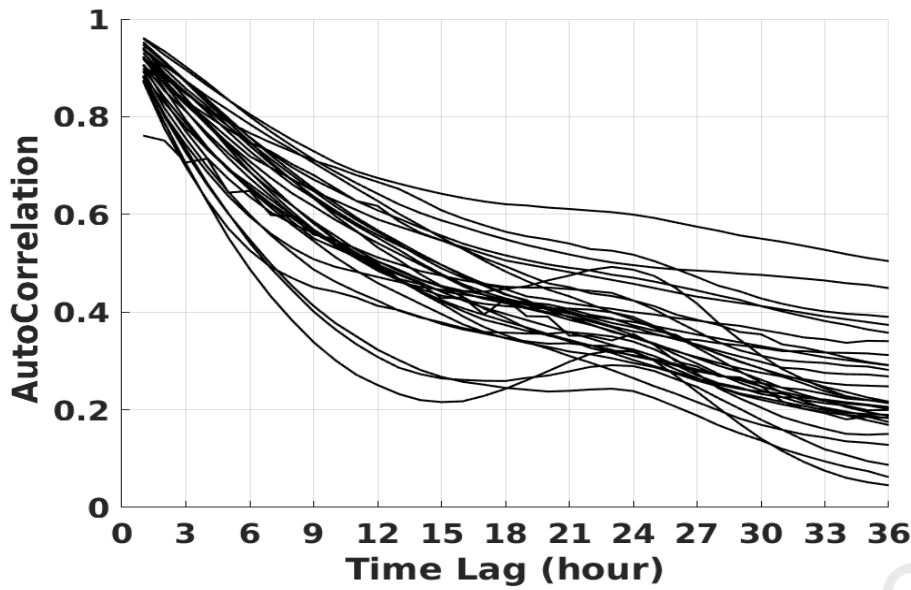
152

153

154

155

Table 1 summarizes the main statistics allowing the characterization of wind speed at each buoy location (Figure 2). As expected, the highest wind speed conditions are found at buoys located northwest of Spain, while the lowest winds are depicted near coast locations or in the Gulf of Cadiz. The three statistical conventional moments (standard deviation (STD), skewness (Skew), and kurtosis (Kur)) indicate that surface wind speed exhibit significant local characteristics. The latter would be further assessed through the estimation of temporal scale variability of wind speed from each buoy. Figure 1 shows the autocorrelation of wind speed as a function time lag varying between 1 hour and 36 hours. It results that most of the wind speeds exhibit significant autocorrelation exceeding 0.80 at 95% confidence level, for time lag lower than 6 hours. Therefore, the satellite surface wind analyses, used in this study, are estimated from remotely sensed data as 6-hourly averages at synoptic times (0000 UTC, 0006 UTC, 0012 UTC, 1800 UTC) over a gridded map of 0.125° in latitude and longitude.



156  
157

158 **Figure 1:** Autocorrelations of wind speeds derived from buoys (Table 1) estimated from all  
159 available hourly measurements.

160  
161

## 162 2.2 WRF model wind estimates

163

164 WRF is a FLOSS (free libre open source software) model, fully compressible and non-hydrostatic,  
165 with a variety of capabilities that meets the needs of both operational forecasting and academic  
166 communities at a variety of spatial scales. It supports multiple dynamical cores, real-data and  
167 idealized simulations, data assimilation capabilities, a broad spectrum of physics and dynamic options  
168 as well as multiple types of nesting [43]. Details of the model setup are summarized in Table 2.

169

170 **Table 2.** WRF system configuration and parameterization options

<b>Horizontal Resolution (km)</b>	9
<b>Temporal resolution (hours)</b>	6
<b>Grid Dimension</b>	96x148
<b>Vertical Grid dimension</b>	47 eta levels
<b>Radiation</b>	CAM scheme for both short and long wave radiation
<b>PBL Physics</b>	Yonsei University scheme
<b>Land Surface</b>	Unified Noah Land Surface Model
<b>Microphysics</b>	WRF Single-Moment 6-class scheme
<b>Cumulus</b>	Kain-Fritsch scheme

171

172 Within the context of this work, WRF version 3.9 was used to downscale the Era-Interim forecasts  
173 with 0.75 degrees of horizontal resolution to a 9 km mesh grid on a 1:3 nesting configuration. The

174 NWP model produces weather data with a 6-hours temporal resolution and 47 vertical levels. The  
 175 computational grid covers the Iberian Peninsula and part of the Atlantic Ocean. Figure 2 illustrates  
 176 the full operational setup of the WRF forecasting system along with the location of the marine buoys  
 177 that supported the quantitative verification of the results.

178



179

180

181 **Figure 2.** WRF domain and location of the offshore buoys from EMODNET database.

182

183

### 184 2.3 Satellite retrieval of surface wind

185

186

The remotely sensed data used in this study is described in various papers (e.g. [44, 45]).  
 187 Satellite data used here are those available during the period 2004 – 2012. The reader may refer to  
 188 the websites, shown in Table 3, providing details about instruments, wind processing, and relevant  
 189 publications and reports. Briefly, the main sources of remotely sensed wind data are from  
 190 scatterometers onboard QuikSCAT (1999 – 2009), Metop-A (2007 – present), and Metop-B (2012 –  
 191 present). Ancillary remotely sensed data are derived from radiometers: Special Sensor Microwave  
 192 Imager Sounder (SSM/I/S) onboard the Defense Meteorological Satellite Program (DMSP) F16 (2003  
 193 – present) and F17 (2006 – present), and from WindSat onboard Coriolis satellite (2003 – present).  
 194 10m wind speed and direction retrievals from SAR onboard Sentinel-1A (2014 – Present) and –1B  
 195 (2016 – Present) are also of concern. They are mainly used for estimating the spatial variation at local  
 196 scales [44].

197

198

Scatterometer and radiometer data used in this study are Level 2 (known as L2b product) wind  
 retrievals available on wind vector cell (WVC) grid within the radar and radiometer ground swath,

199 i.e., suitable areas (depending on radar/radiometer characteristics). Scatterometer and WindSat  
200 provide both wind speed and direction at 10m height, while SSMI/S provide only 10m wind speed.  
201 The WVC grid size varies among different wind products. QuikSCAT WVC grids are of 12.5 km x  
202 12.5 km, while ASCAT WVC is of 25 km x 25 km until 2009, and of 12.5 km x 12.5. Scatterometer  
203 beams measure the normalized radar cross-section (NRCS), also known as backscatter coefficient  
204 ( $\sigma^0$ ), from the wind-roughened sea surface, which is mainly a function of wind condition (speed and  
205 direction). Backscatter  $\sigma^0$  data represent a dimensionless property of the surface, describing the ratio  
206 of the effective echoing area per unit area illuminated. Scatterometer wind retrievals are obtained  
207 from  $\sigma^0$  measurements through an inversion procedure based on the use of Geophysical Model  
208 Functions (GMF). Scatterometer wind retrievals are provided over swaths of 1800km (QuikSCAT),  
209 and 2×600km (ASCAT). The links shown in Table 3 provide technical details related to scatterometer  
210 wind processing. References such as [42; 44] provide results related to the accuracy of scatterometer  
211 wind retrievals.

212 The ancillary remotely sensed wind data used in this study are retrieved from the special sensor  
213 microwave imager (SSM/I) and sounder (SSMIS) brightness temperature measurements ( $T_B$ ). Only  
214 surface wind speed at 10m height can be derived from SSMI and SSMIS  $T_B$  based on the use of an  
215 empirical model fitting the relationship between surface wind speed and  $T_B$  through the radiative  
216 transfer equation (RTE). They are provided by a remote sensing system (RSS) [46]. SSM/I and  
217 SSMIS wind data are available over swath (1400 km width) at wind cell of  $0.25^\circ$  in latitude and  
218 longitude over global oceans.

219 Sentinel-1A and -1B SAR wind speed and direction retrievals, used in this study, are known as  
220 level 2 ocean (L2OCN) products, acquired in interferometric wide (IW) swath mode. Data are  
221 available over a swath of 250 widths, with a moderate geometric resolution of  $5 \text{ m} \times 20\text{m}$ . Details  
222 about SAR winds and the related accuracy are available in the literature [44].

223 Several publications provide useful information related to improving the accuracy of the  
224 remotely sensed winds (see for instance [47]). For this study, the accuracy, at the regional scale, of  
225 the remotely sensed winds is briefly assessed through comprehensive comparisons with buoy  
226 measurements used in this study. To achieve the comparison, buoy and satellite wind retrievals are  
227 collocated based on the spatial and temporal criteria, 25 km and 1 hour, respectively. Table 4  
228 summarizes some statistical parameters aiming at the characterization of the comparisons of buoy  
229 and satellite retrieval wind speeds, zonal components, and meridional components. The resulting  
230 statistical parameters shown in table 4 are also required for the calculation of blended winds (see  
231 hereafter).

232

233

**Table 3:** Relevant websites providing information about radars and radiometers used in this study.

Satellite	Period	Website
QuikSCAT	1999 – 2009	<a href="https://podaac.jpl.nasa.gov/dataset/QSCAT_LEVEL_2B_O WV_COMP_12">https://podaac.jpl.nasa.gov/dataset/QSCAT_LEVEL_2B_O WV_COMP_12</a> ,
ASCAT	2006 – Present	<a href="projects.knmi.nl/scatterometer/ascat_osi_12_prod">projects.knmi.nl/scatterometer/ascat_osi_12_prod</a>
SSMIS F16	2003 - Present	<a href="http://data.remss.com/ssmi/f16/bmaps_v07/">http://data.remss.com/ssmi/f16/bmaps_v07/</a>
SSMIS F17	2007 - Present	<a href="http://data.remss.com/ssmi/f17/bmaps_v07/">http://data.remss.com/ssmi/f17/bmaps_v07/</a>
WindSat	2003 - Present	<a href="http://data.remss.com/windsat/bmaps_v07.0.1/">http://data.remss.com/windsat/bmaps_v07.0.1/</a>
Sentinel SAR	2014 - Present	<a href="https://sentinel.esa.int/web/sentinel/missions/sentinel-1/data-products">https://sentinel.esa.int/web/sentinel/missions/sentinel-1/data-products</a>

**Table 4:** Comparison of statistical parameters of collocated 10m wind speed, zonal, and meridional components from buoys and QuikSCAT, ASCAT retrievals, and WRF model analyses for 2004 – 2012. Bias is defined as the mean difference between buoy and product winds (in this order). RMS,  $b_s$ ,  $a_s$ , and  $\rho$ , indicate root mean difference, regression coefficients (slope and intercept), and scalar correlation coefficient, respectively. Length is the number of collocated buoy and satellite wind data. Similar statistics are also shown for Sentinel-1a SAR IW winds. The former is estimated from buoy and SAR collocated data for 2015 – 2018.

	Wind Speed					
	Length	Bias (m/s)	RMS (m/s)	$b_s$	$a_s$ (m/s)	$\rho$
QuikSCAT	29911	-0.17	1.39	0.90	0.72	0.95
ASCAT	18252	0.06	1.27	0.91	0.57	0.95
SAR	3887	0.45	1.65	0.86	0.49	0.91
Zonal wind component						
QuikSCAT	29390	0.21	2.54	1.20	-0.20	0.92
ASCAT	18115	0.03	1.66	1.15	-0.02	0.96
SAR	3719	0.13	1.83	1.07	-0.12	0.93
Meridional wind component						
QuikSCAT	29572	-0.50	2.21	1.14	0.38	0.91
ASCAT	18080	-0.13	1.68	1.15	-0.02	0.96
SAR	3787	-0.42	2.04	1.05	0.37	0.92

234

235

236

237

238

239

240

The resulting statistics (Table 4) are determined assuming that buoy and satellite winds are both non-error-free. Only those obtained for scatterometers QuikSCAT and ASCAT are shown. Both are similar to those obtained from scatterometer accuracy determination based on the use of buoy networks such as National Data Buoy Centre (NDBC) and Météo-France and U.K. Met Office buoys [48]. Biases are small, RMS wind speed differences do not exceed 1.40 m/s, and correlation exceeds 0.90 at 95% confidence. RMS differences of QuikSCAT zonal and meridional wind components

241 exceed 2 m/s, while those estimated for ASCAT are about 1.70 m/s. It results from the difference in  
 242 collocated buoy/QuikSCAT and buoy/ASCAT low wind speed (<5 m/s) distributions. They account  
 243 for almost 27%, and 22% of the total length of collocated data, respectively. Excluding wind speeds  
 244 lower than 5 m/s, lead to similar statistics for QuikSCAT and ASCAT wind components (not shown).

245 Table 4 also shows statistics aiming at the characterization of the comparison between a buoy  
 246 and SAR IW winds. They are only required for the determination, from SAR IW retrievals, of the  
 247 spatial structures of surface wind speed, zonal, meridional wind components along the area of interest  
 248 (see section 2.4). Buoy and SAR IW agree well. However, SAR IW wind speed tends to be  
 249 underestimated compared to buoy measurements [49]. Briefly, it relies on GMF used for retrieving  
 250 wind speed and direction from the SAR backscatter coefficient.

251

## 252 2.4 Blended WRF and satellite wind fields

253

254 The method aiming at the determination of regular space and time surface wind fields, named  
 255 surface wind analyses, over the oceanic area of interest, from remotely sensed observations, is  
 256 described in previous papers (e.g. [49]). It is an objective method based on the kriging technique with  
 257 the external drift method as described in the aforementioned reference. External drift is from the WRF  
 258 model. Briefly, the scatterometer and radiometer winds are used to estimate 6-hourly averaged wind  
 259 speed and direction over all grid cells of  $0.125^\circ$  in latitude and longitude (except grid cells over land).

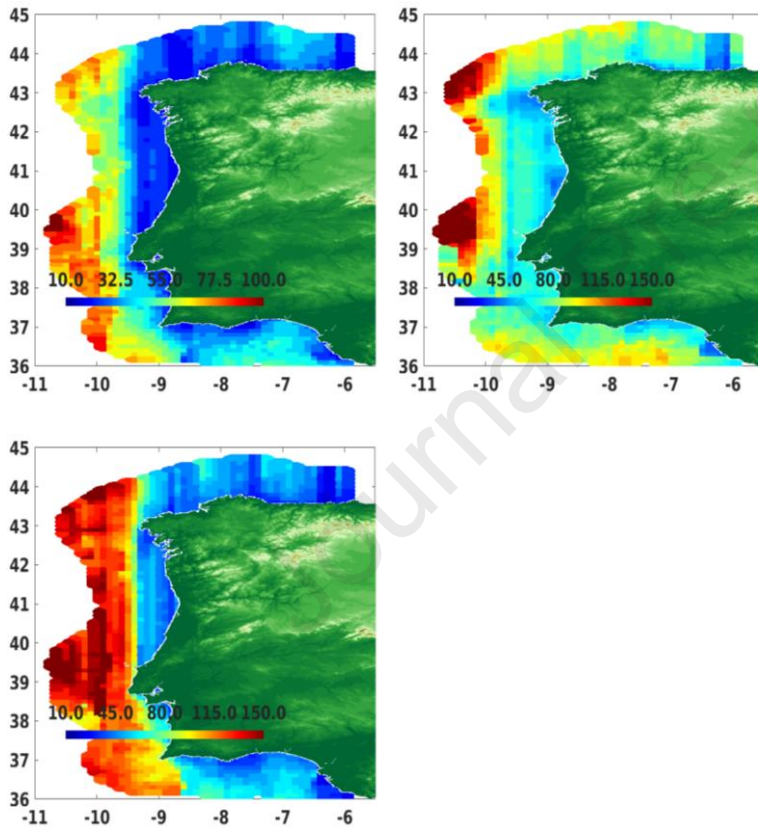
260 The contribution of each remotely sensed data requires knowledge of the associated weight.  
 261 The latter accounts for the spatial and temporal separations of the analysis. Weight determination  
 262 requires the knowledge of the spatial and temporal variability function (named variogram) of wind  
 263 speed, zonal, and meridional components. Variograms illustrate the spatial and temporal scales of the  
 264 variable, which are highly related to the space and time covariance functions. In practice, the  
 265 variogram is determined as a parametric function, requiring the determination of three parameters.  
 266 Two parameters, called variogram spatial and temporal ranges, indicate respectively the spatial and  
 267 temporal lags beyond where no significant spatial and temporal correlation between wind variables  
 268 are drawn. The third parameter (called sill) is the variogram value associated with the variogram  
 269 ranges.

270 Figure 3 shows the spatial scales (in km) of wind speed of the related wind components. They  
 271 are determined from SAR IW retrievals based on the use of the method described in [45]. Briefly,  
 272 for each hour of the day and each point on a  $0.125^\circ \times 0.125^\circ$  grid, SAR-based wind covariances are  
 273 estimated as a function of distance  $\delta h$  for  $1 \text{ km} \leq \delta h \leq 300 \text{ km}$  at 5 km steps. The hourly statistics is  
 274 estimated only if the sampling length of SAR retrievals is significant ( $\geq 30$ ). Space distribution of the  
 275 spatial scales reflects the nature of local air–sea–land interactions and generally aligns with local

276 topography. The presence of sharp landmasses (such as capes) would introduce apparent  
 277 inhomogeneities to spatial scale maps. Local air–sea–land interactions are also reflected in the spatial  
 278 distribution of wind scale patterns that tend to be aligned with regional coastal configuration and  
 279 topography.

280 Wind speed (Figure 3a) exhibits small spatial scales, laying between 10km and 30km, over  
 281 coastal areas (<100 km of coastlines), while over offshore areas, these scales are mostly higher than  
 282 50km. As expected, regarding spatial wind patterns, the coastal wind speed scale exhibits a significant  
 283 zonal pattern. Similar results are found for the zonal wind component (Figure 3b) and meridional  
 284 wind component (Figure 3c). However, their spatial scales are larger than those found for wind speed  
 285 and generally exceed 30km, except at a few locations.

286

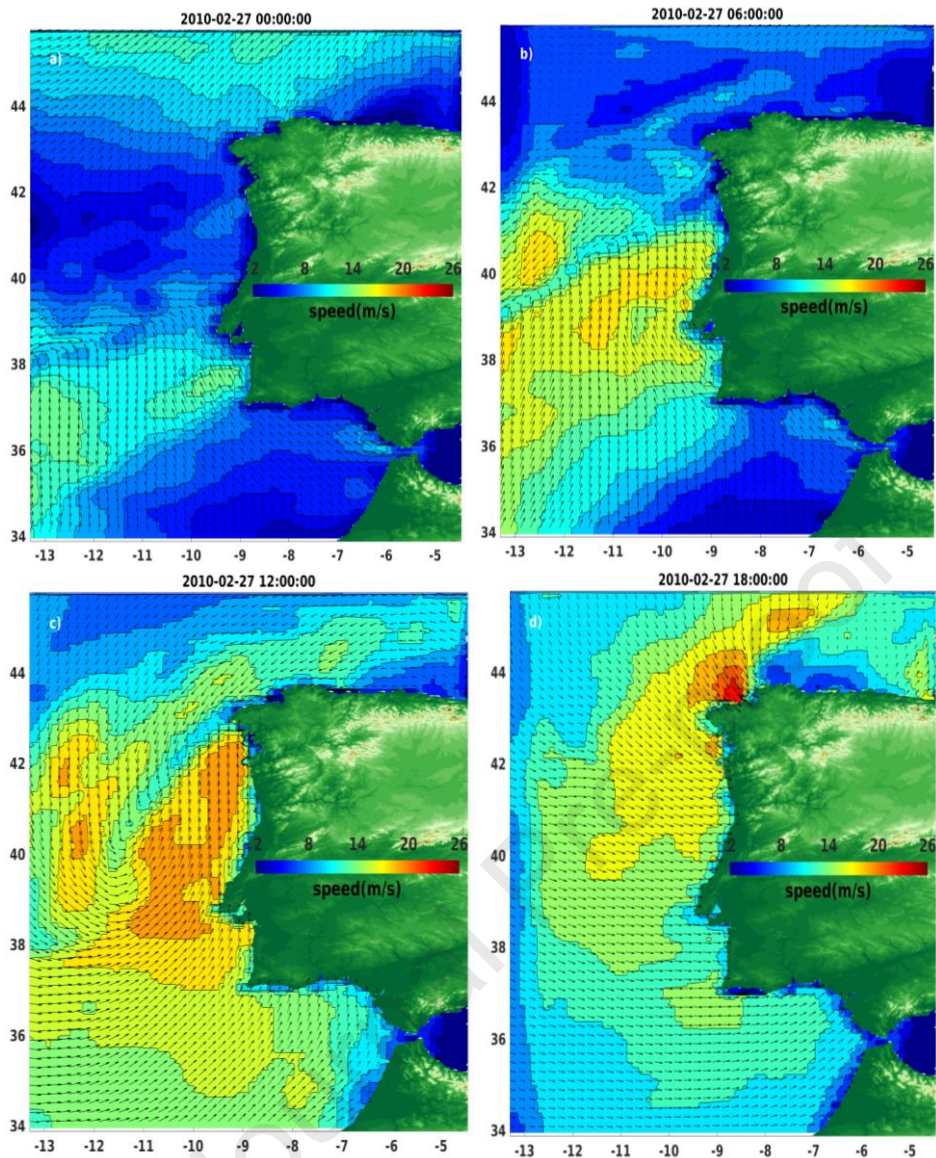


287

288 Figure 3: Spatial wind patterns of a) wind speed (m/s), b) zonal wind component (m/s), and c) meridional  
 289 wind component (m/s), estimated from Sentinel SAR wind retrievals. They are determined at each grid cell  
 290 ( $0.125^\circ \times 0.125^\circ$ ) off Portugal and Spain's Atlantic coasts. The x-axis and y-axis represent the longitude and  
 291 latitude of the domain. The colour shows the spatial scale value (in km)

292

293 The determination of the variogram temporal range is based on the use of the results drawn  
 294 from the buoy temporal autocorrelation behaviours (Figure 1). The former indicates that the wind  
 295 temporal scale would be lower than 12 hours.



296

297 Figure 4: Examples of four consecutive 10m blended satellite wind analyses occurring on 27  
 298 February 2010 at the synoptic time a)00h:00, b)06h:00, c)12h:00, and d)18h:00 UTC. The x-axis  
 299 and y-axis represent the longitude and latitude of the domain. Colour indicates wind speed values,  
 300 while the black arrows indicate wind direction.

301

302

303

304

305

306

307

308

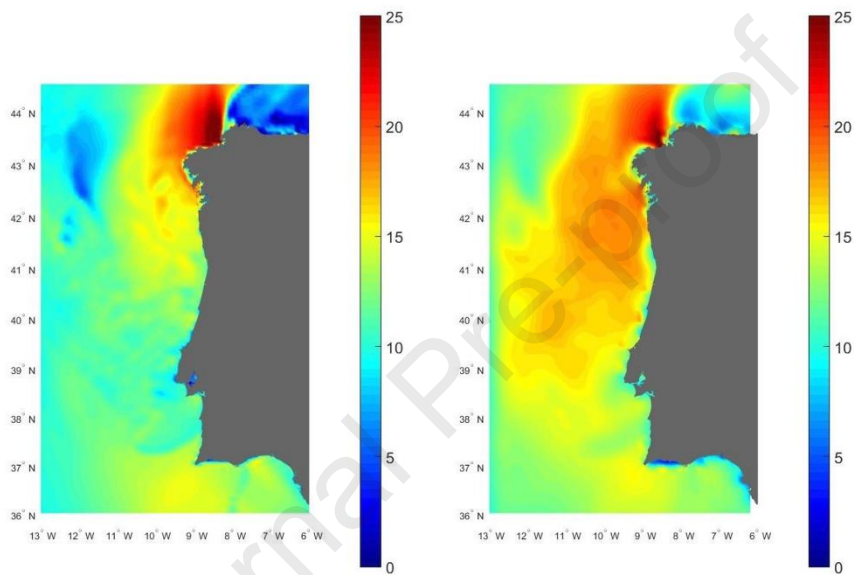
309

The resulting variograms are then used as inputs of the objective method components aiming  
 at the determination of regional satellite wind analyses at synoptic times. The latter is also referred to  
 as blended satellite winds or 6-hourly satellite wind analyses. An example of these wind analyses is  
 shown in Figure 4. It shows four consecutive 6-hourly analyses of 27 February 2010. It assesses the  
 spatial and temporal variability of wind speed as well as wind direction, associated with southeast-  
 northeast high wind condition development.

Figure 5 shows an example of the differences across the two datasets, the WRF and blended  
 winds, for the strong wind episode occurring on February 27<sup>th</sup>. It can be seen that the WRF model

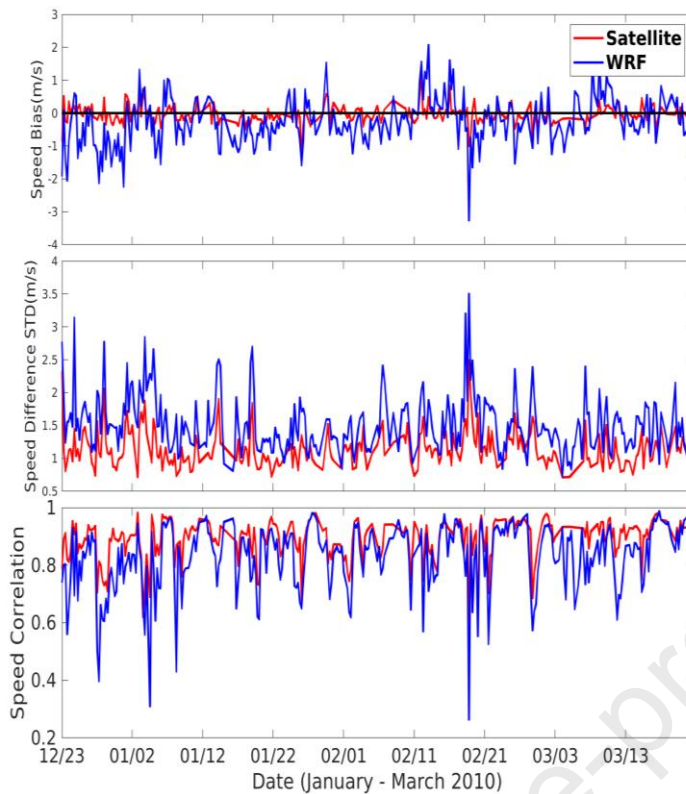
310 can reproduce the wind pattern generally well. Areas of increased wind speed in the northwest corner  
 311 are visible in both maps although it is clear that WRF underestimates high wind speeds between the  
 312 37° and 43° parallels. The general tendency for WRF to underpredict strong winds is well known and  
 313 has previously been discussed [39]. In contrast, across the area of the highest concentration of strong  
 314 winds, at the northwest corner of Galicia, WRF overestimates the maximum observed winds. This  
 315 was confirmed by comparison with buoy measurements in that area not presented in this section. The  
 316 use of the blended product allows correcting the model bias further improving the accurate  
 317 reproduction of the local meteorological phenomena.

318



319  
 320 Figure 5: Example of the difference between WRF 10m wind speed (left) and blended wind maps  
 321 for the high wind episode occurring on 27 February 2010 at synoptic time 18:00.  
 322

323 The resulting satellite 6-hourly analyses are first compared to remotely sensed wind data. It  
 324 assesses the ability of satellite analyses to restore the observed surface wind characteristics. To  
 325 achieve such comparisons, satellite wind analyses and WRF wind estimates are collocated in space  
 326 and time with satellite observations. The collocation spatial and temporal criteria are 25km, and  
 327 3hours, respectively. Figure 6 shows the time series of statistical parameters (mean difference (bias),  
 328 the standard deviation of the difference, and correlation), estimated at a regional scale, aiming the  
 329 characterization of the comparison between satellite wind speed observations and, on one hand,  
 330 satellite analyses, and on other hand WRF estimates. It is concluded that satellite wind analyses  
 331 improve the results of the comparisons. Indeed, Bias as STD is reduced and correlation increases,  
 332 compared to results found for WRF.



333

334 **Figure 6:** Time series (January 1<sup>st</sup> - March 31<sup>st</sup>, 2010) of statistical parameters (mean (bias) (panel  
 335 on top) and standard deviation (STD) (middle) wind speed difference, and the related correlation  
 336 coefficient (in bottom)) characterizing the comparisons between satellite wind speed observations  
 337 and analyses (shown in red color), and between satellite wind speed observations and WRF estimates  
 338 (in blue color)  
 339

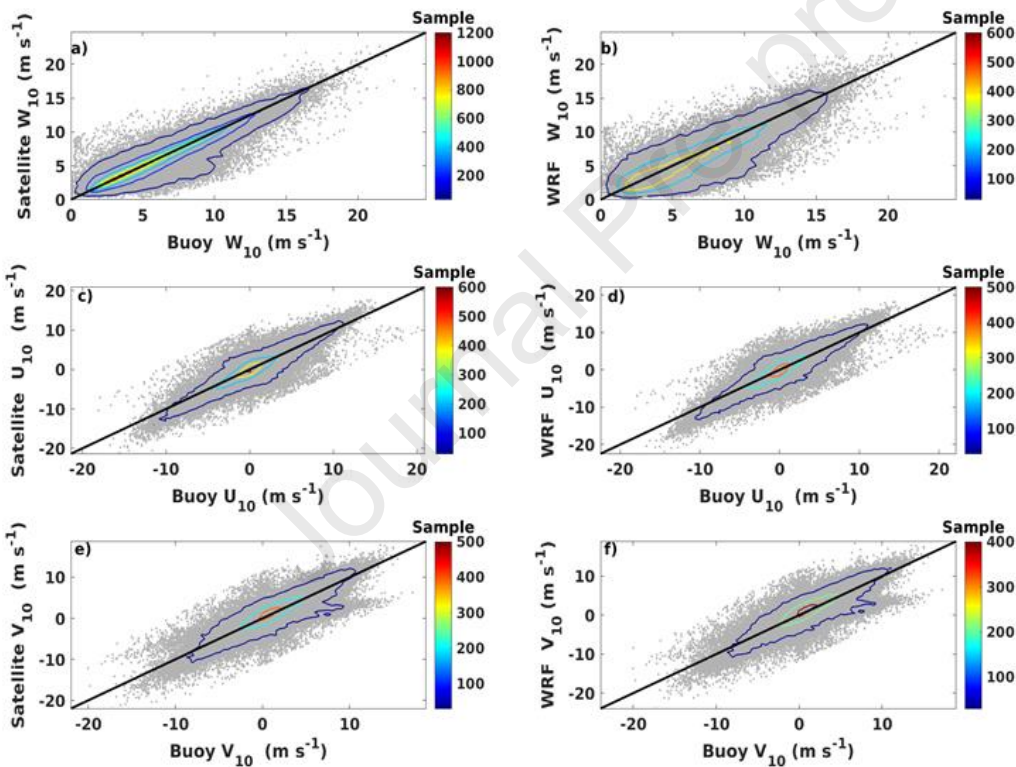
340 Nine years (2004 – 2012) of satellite wind analyses are calculated. Their accuracy is determined  
 341 through comprehensive comparisons with 6-hourly averaged buoy (Table 1) wind speed and  
 342 direction. The latter is estimated from valid 10m hourly wind data available within 3 hours of synoptic  
 343 times. Only 6-hourly buoy data estimated at least with 3 hourly measurements are selected for  
 344 comparison purposes. Buoy and satellite 6-hourly winds available at the same synoptic times and  
 345 located within 12.5 km of each other, are selected as collocated data, and used for the determination  
 346 of satellite analysis accuracy. A similar procedure is used for collocating in space and time buoy and  
 347 WRF winds.

348 Figure 7 shows a comparison between buoy and satellite (left column panels) and between  
 349 buoys and WRF (right column panels). Both WRF and satellite exhibit good agreement with buoy  
 350 data. However, satellite analysis improves the comparisons, especially for wind speed (Figure 7 a)  
 351 and b)). The scatter of the satellite wind speed analysis is reduced for almost all wind speed ranges.  
 352 More specifically, the RMS of the difference between buoy and satellite, and between buoy and WRF  
 353 are 1.71 m/s, and 1.97 m/s, respectively. Although satellite zonal (Figure 7 c)) and meridional (Figure

354 7 e)) wind components exhibit better comparison results, compared to WRF results (Figure 7 d) and  
 355 f)), the improvements are quite limited. For instance, the RMS difference values of the zonal  
 356 component are 2.06 m/s and 2.19 m/s for satellite and WRF, respectively (Figure 8).

357 It is worth mentioning that the performance metrics presented here are in-line with those  
 358 published in similar studies. Other authors compared WRF simulations against the same network of  
 359 buoys used in this work, obtaining analogous results for the same statistical scores [36]. Similarly,  
 360 the authors in another study obtained analogous RMSE values in comparisons of WRF against 8 mast  
 361 and lidar sites across northern Europe [50]. This is an important result since these were the results of  
 362 the validation that preceded the creation of the New European Wind Atlas. Still, WRF model has been  
 363 tuned and tested in the region that motivated this study turning it into a better choice for on-site  
 364 resource assessment.

365

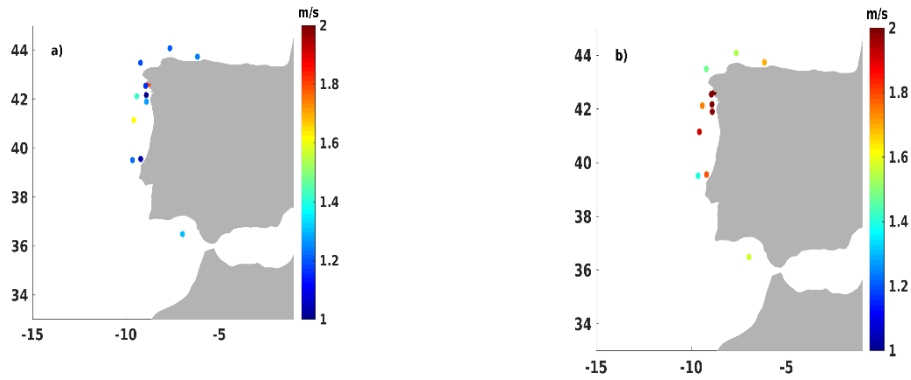


366

367 **Figure 7:** comparison of 6-hourly buoy and satellite analyses (left column), and between buoys and  
 368 WRF (right column). Panels in the top (a) and b)), middle (c) and d)), and bottom e) and f)) show  
 369 wind speed, zonal, and meridional comparisons, respectively. Coloured contours indicate the  
 370 sampling length of collocated data associated with wind bins of  $0.5 \text{ m s}^{-1}$  width. Only contours  
 371 associated with sampling length exceeding 30 are shown.

372

373



374 **Figure 8:** Root mean square differences (RMSD) between buoy and satellite (a), and between  
 375 buoys and WRF wind speed (b), shown at buoy locations.

376  
 377

### 378 **3 Validation of the dataset**

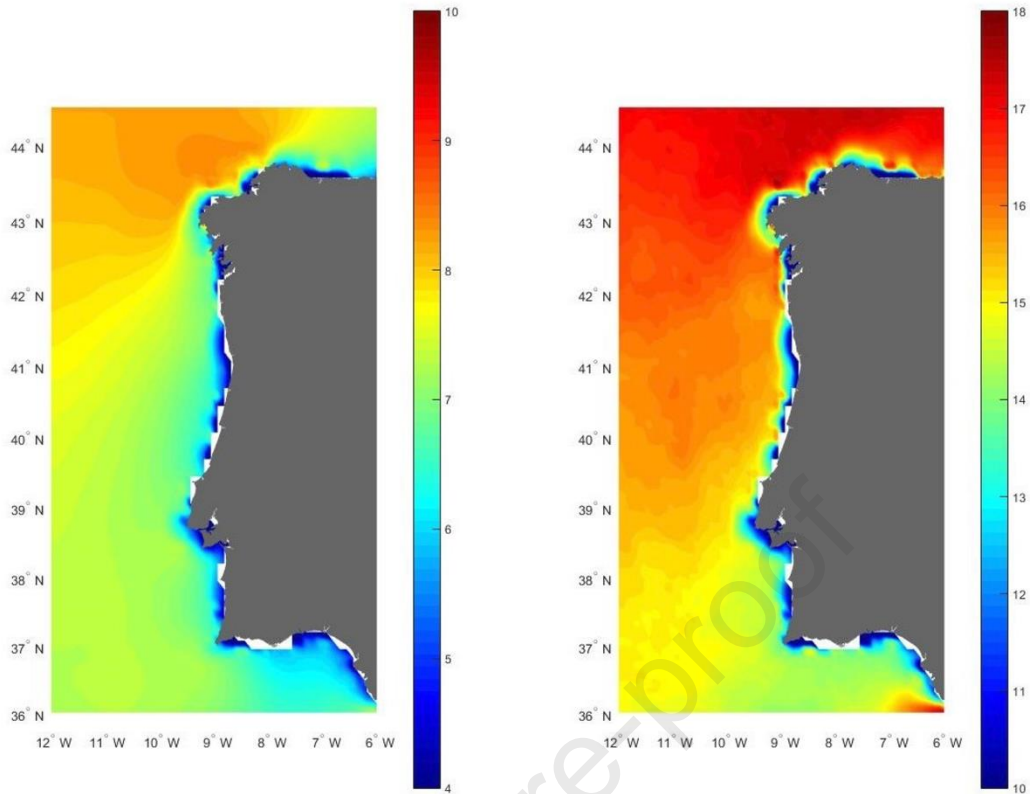
#### 379 **3.1 Wind speed**

380

381 In this section, the spatial and temporal wind patterns are analyzed in more detail using the blended  
 382 winds described in the previous section. To gain further insight into the spatial pattern of the mean  
 383 wind speed, a wind map is drawn and displayed in Figure 9 (left panel). As it is observed, two main  
 384 characteristic patterns are evident from the colour distribution analysis. The wind speed is higher in  
 385 the northern regions, most particularly in the northwest corner of the Iberian Peninsula, where wind  
 386 speed is above 8.5 m/s on average.

387 This region of Galicia is affected by strong west winds that come from the Atlantic low-pressure  
 388 systems. As expected, winds rapidly increase with the distance to the coast varying between 5-6 m/s  
 389 along the western coast and rapidly increasing up to 8.5 m/s in the northern regions. In the south, the  
 390 lowest wind speeds occur, with magnitudes of around 4-5.5 m/s near the coast though they still  
 391 represent attractive conditions for wind projects. Overall, winds vary between 6-7.5 m/s in the west  
 392 side of the Iberian Peninsula, most affected by western Atlantic winds, indicating good overall  
 393 conditions for building wind parks taking into account the average water depth and distance to shore  
 394 of offshore wind farms [51].

395 In addition to the annual means, extreme winds are calculated using the statistical percentile  
 396 procedure (Figure 9, right panel). In this paper, the threshold chosen to define the extremes was the  
 397 99th percentile. The map at the upper percentile level (right panel of Figure 9) shows that the lowest  
 398 extreme winds occur in the south, not exceeding 14 m/s on average. This is also valid near the coast  
 399 throughout most of the domain, though rapidly increasing up to 17 m/s in the northmost regions and  
 400 with the distance from the coast. This is suitable for most wind turbines which have a typically rated  
 401 speed of 11-17 m/s and cut off speed of 25 m/s. [52-53].

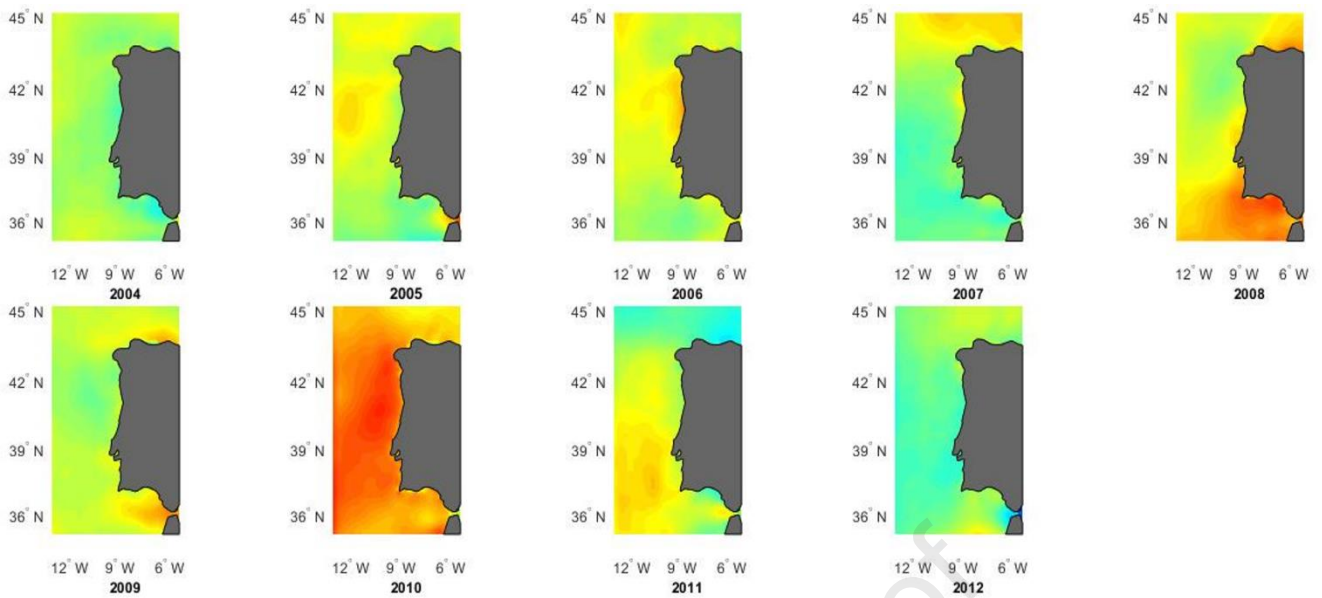


402 **Figure 9:** Annual average 10m blended wind speed (m/s) for the 9-year period (left) and 99th  
 403 percentile (right).  
 404  
 405  
 406

### 407 3.2 Annual wind variability

408  
 409 To access the inter-annual variability, Figure 10 shows the normalized wind speed from 2004 to  
 410 2012. The deviations from the mean are calculated by dividing each year's average wind speed records  
 411 by long-term mean throughout the 9 years  $u = U/\bar{U}$ . These numbers allow analysing the variability  
 412 for the 9 years and to estimate the deviations from the long term mean value during that period.

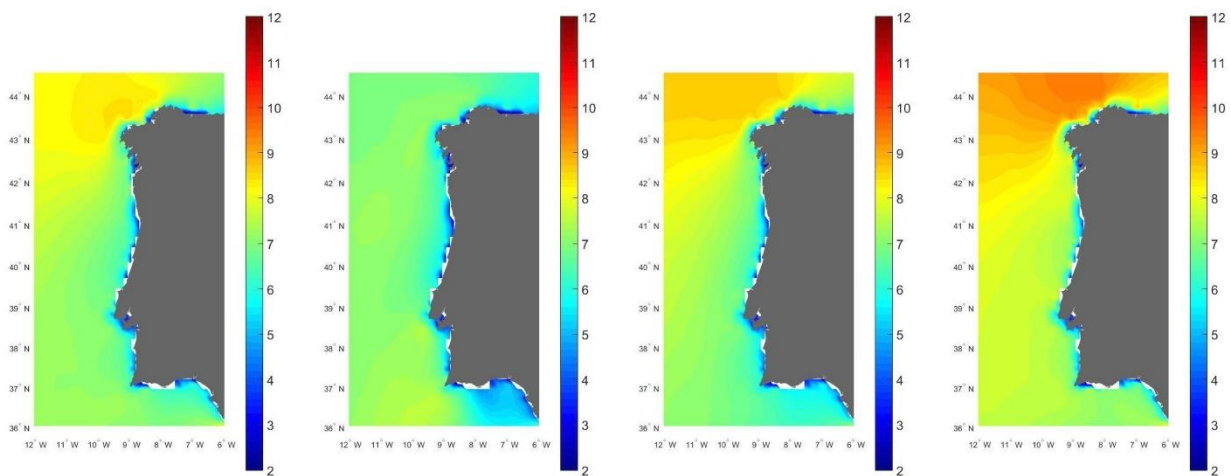
413 The results show that the annual wind speed ranges from a low of 85-90% of the 9-yearly mean  
 414 wind speed to a high of 125% of the average intensity. An increasing trend is noticed throughout 2010  
 415 though preceded by lower the intensity year of 2009. According to the wind analysis, the years 2008  
 416 and 2010 show the higher average intensity up to nearly 115% of the medium-term mean contrasting  
 417 with the years of 2004 and 2007 that show lower intensity winds. For the year 2010 in particular, the  
 418 distinct pattern is likely related to the strong signature of North Atlantic Oscillation [54]. These maps  
 419 give a general overview of the spatial and temporal patterns of the wind in the selected region,  
 420 however, a thorough analysis must be done in specific regions for wind turbine implementation.  
 421



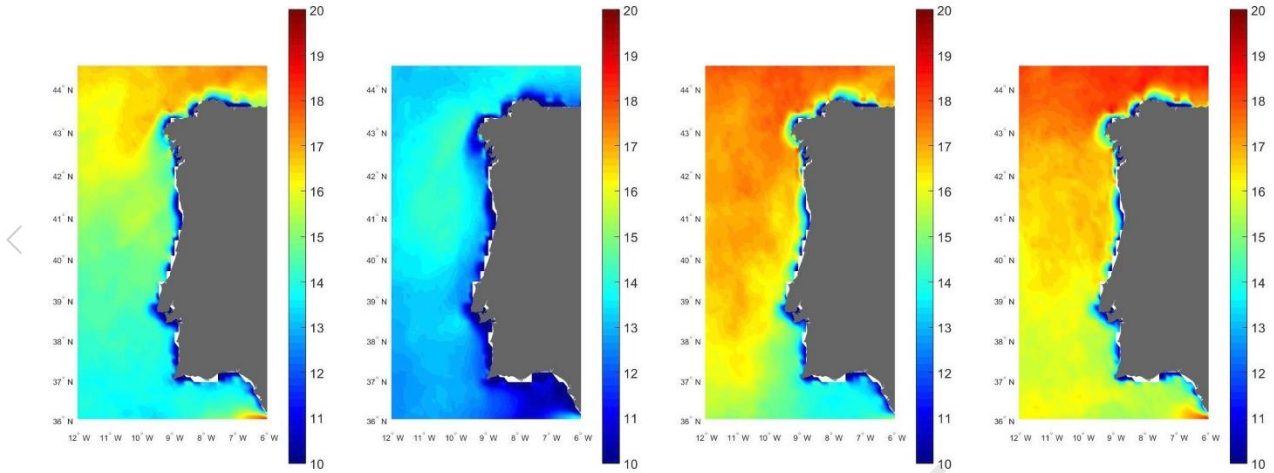
422  
423 **Figure 10:** Normalized wind speed (m/s) for 2004-2012. The deviations from the mean are calculated  
424 by dividing each year average wind speed records by the 9-yearly mean wind speed  $u = U/\bar{U} * 100$ .

### 425 3.3 Seasonal wind variability

426  
432 The seasonal distribution of winds for the study area is shown in Figure 11. As expected, the winter  
433 represents the most energetic season with winds of greater magnitude occurring more frequently,  
434 especially above the 7 m/s threshold and exceeding 9 m/s in the northern regions. Conversely, lower  
435 magnitude winds occur more frequently in the spring and summer even though the difference is more  
436 noticeable in the northwest corner of the domain. Along the coast, winds still exceed on average 6  
437 m/s which still represents attractive conditions. This is due to the strong winds that occur during  
438 summer in Portugal, created by a thermal low over the Iberian Peninsula and the Azores high-pressure  
439 system [55]. These blow mostly from North-Northeast directions and contribute to the potential for  
440 wind exploitation during these months.



441  
442 **Figure 11:** Wind speed seasonal variations (m/s). From left to right (spring, summer, fall, winter)  
443



444  
445 **Figure 12:** 99<sup>th</sup> percentile wind speed (m/s). From left to right (spring, summer, fall, winter)

446  
447 Figure 12 shows the spatial distribution of winds exceeding the 99<sup>th</sup> percentile. The winds exhibit  
448 similar spatial characteristics to the average wind displayed in Figure 11. Overall, extreme winds  
449 range from 11-19 m/s over the selected domain throughout the year. All seasons have their largest  
450 winds in the northwest corner of the domain, in agreement with the median wind maps. Similarly,  
451 summer is the period with the lowest magnitude winds. It is also interesting to notice that for the  
452 winter and fall seasons, the spatial distribution of the extreme wind differs in how it compares with  
453 the median wind pattern. Although the winds are stronger on average during the winter season  
454 between the 37 and 41° parallels, fall months are subject to larger magnitude extreme winds in this  
455 subsection of the domain.

456  
457

#### 458 **4 Wind Energy**

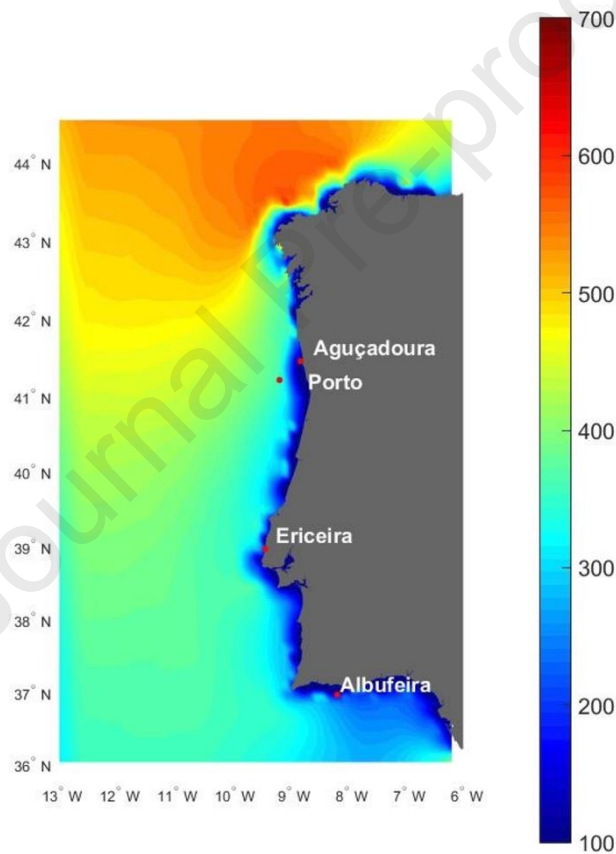
459  
460 One of the potential benefits of an accurate wind product is an accurate estimation of wind energy.  
461 The energy resources at selected regions of interest have been determined using the blended wind  
462 product. The wind power density (WPD) is calculated over the entire area and further in detail for the  
463 three proposed locations for wind turbine implementation. The wind power density is calculated  
464 considering the wind speed frequency of occurrence in 1 m/s intervals, using the following  
465 expression:

$$466 \quad WPD = \frac{1}{2} \rho v^3 \quad WPD = \frac{1}{2} \rho v^3 \quad (6)$$

467 where the air density  $\rho$  (kg/m<sup>3</sup>) is taken as 1.225 kg/m<sup>3</sup>.

468 From the seven wind power classes defined [56], class 3 and above are considered suitable for most  
469 wind power projects. This corresponds to a WPD of 150/200 W/m<sup>2</sup> at 10 m height or the equivalent

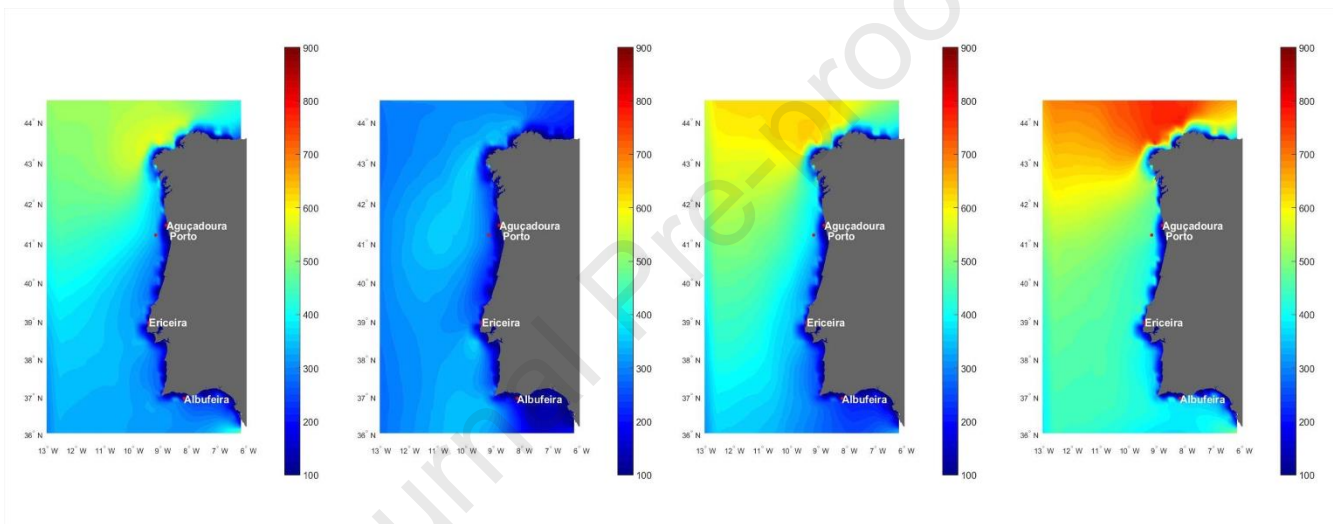
470 5.1/5.6 m/s mean wind speed. Figure 13 shows the spatial pattern of the wind power density obtained  
 471 from the satellite analyses. The northern region denotes the highest potential while the southern areas  
 472 have more modest values available for exploitation. Still, there is an overall high amount of energy  
 473 along the entire coast with great dependence upon the distance to the coast. Nearly 350-400 W/m<sup>2</sup>  
 474 (class 6) are available in average for extraction offshore the north and central coast and 250-300  
 475 W/m<sup>2</sup>.  
 476 The pronounced seasonal variations of the energy density in the Iberian Peninsula offshore area are  
 477 depicted in Figure 14. Three sites are marked to identify the most energetic region across the country.  
 478 Porto, Ericeira and Albufeira are some of the potential sites, a choice that was based on a preliminary  
 479 inspection of physical and environmental limitations among other constraints [57].



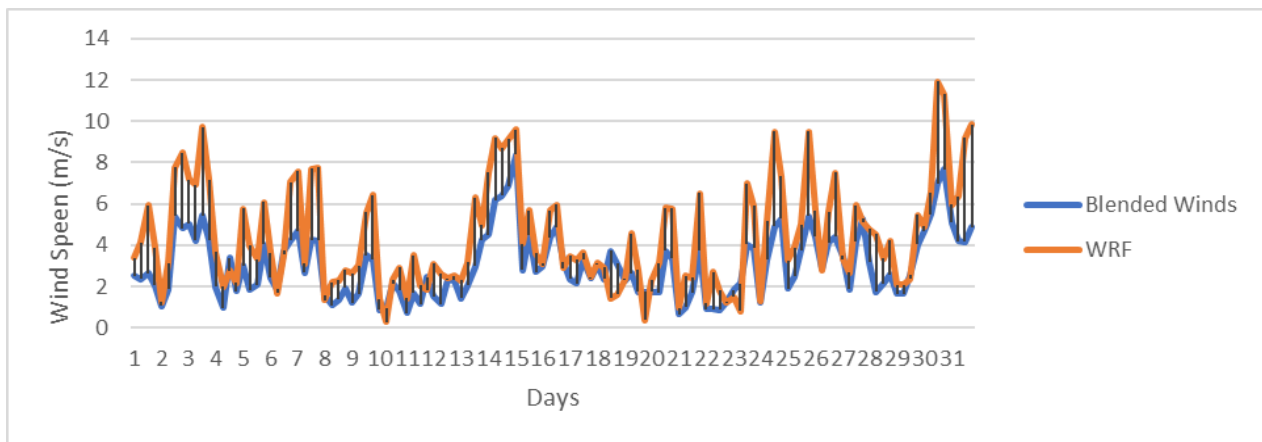
480  
 481 **Figure 13:** Average Wind power density (W/m<sup>2</sup>) in the Iberian Peninsula coast from 2004-2012;  
 482 winds obtained from the satellite analyses.  
 483  
 484 The maps illustrate how the winds are maximum during winter months and less intense during the  
 485 rest of the year in agreement with what was presented in subsection 3.4. Summer is the least energetic  
 486 season, but the potential progressively increases until it reaches its maximum value during the winter  
 487 season. In terms of overall potential, the values vary around 300-600 W/m<sup>2</sup> during the winter season

488 decreasing to 100-300 W/m<sup>2</sup> during the summer. It is interesting to notice that during summer the  
 489 spatial variability is remarkably decreased when compared with the other seasons. Still, even during  
 490 the least energetic seasons, the observed potential corresponds to a wind class 5.

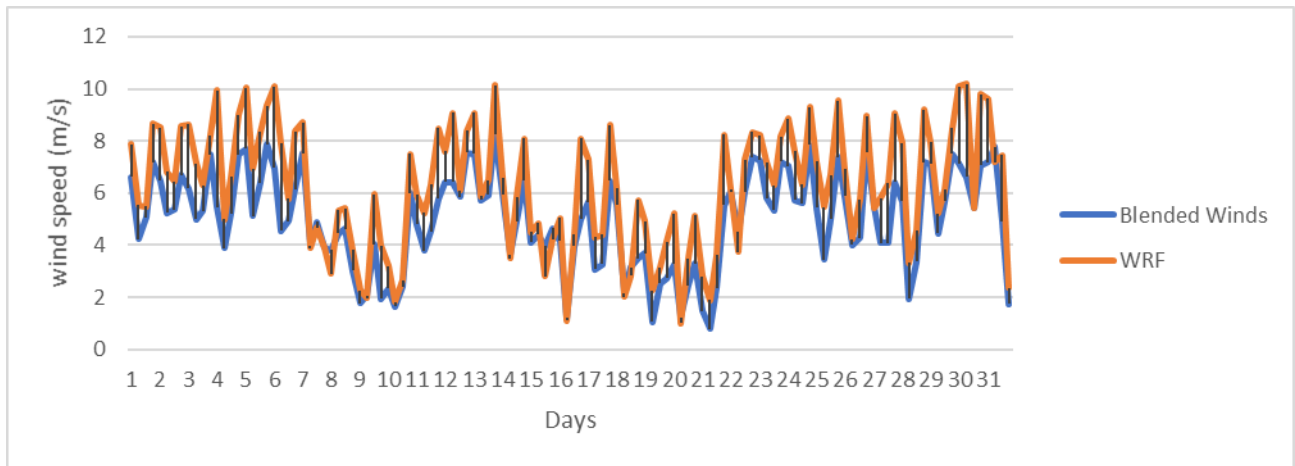
491 Figures 15 and 16 show the 10m wind speed time series for two wind energy test sites. The two  
 492 datasets are compared: wind data obtained from WRF model and the new blended winds.  
 493 Additionally, the results obtained from wind speed derived from the new European wind atlas is also  
 494 summarized in table 5. Figures 16 and 17 show a generally good agreement between the two datasets  
 495 as expected though WRF derived winds are consistently higher throughout the year which can lead  
 496 to an overestimation of the available resource at a particular site. In addition, an inspection of table  
 497 5, shows that even a small difference in the average wind speed can translate into power density  
 498 differences of roughly 200 W/m<sup>2</sup> annually. The opposite is also true.



499  
 500 **Figure 14:** Wind power density seasonal variations (W/m<sup>2</sup>). From left to right (spring, summer, fall,  
 501 winter)  
 502  
 503



504  
 505 **Figure 15.** 10m wind speed (m/s) offshore Aguçadoura during the month of August of 2012  
 506



507  
508 **Figure 16.** 10m wind speed (m/s) offshore Albufeira during August of 2012

509  
510 **Table 5.** Mean Wind speed and power density values for two selected wind energy test sites

Source	Area	Aguçadoura	Albufeira
WRF	Wind Speed (m/s)	4.10	6.34
	WPD (W/m <sup>2</sup> )	243	278
Blended data	Wind Speed (m/s)	5.74	5,31
	WPD (W/m <sup>2</sup> )	459	285
Wind Atlas	Wind Speed (m/s)	5.48	5.90
	WPD (W/m <sup>2</sup> )	214	220

511  
512  
513 As an example, at Albufeira, despite the similar average wind power density estimated for the year  
514 2012, the average wind speed differs by only 1 m/s. But oppositely, at Aguçadoura, 1.6 m/s difference  
515 in the average wind translate into nearly 200 W/m<sup>2</sup> of available power while 0.3 m/s difference from  
516 the wind Atlas dataset derived wind, in turn, would mean an additional 250 W/m<sup>2</sup> yearly. Looking at  
517 the wind Atlas annual values we can see they are quite similar even though the two regions have  
518 considerable differences in the actual wind resource. To give an example of the implications of such  
519 differences, at Albufeira considering the WRF results, a wind turbine with a cut-in wind speed of 4  
520 m/s would operate 354 days per year while using the blended winds the forecast is 339 working days.  
521 This has strong implications, especially when assessing a realistic maximum yield of offshore wind  
522 as the numbers will dictate investment needs and designing strategies to maximize the net energy  
523 flux. If we take into account the validation of the blended winds, and consider them accurate, this will  
524 affect the wind energy projections. Still, a comparison with observations such as buoy or mast data  
525 would be of utmost importance in the initial stages of a wind project.

526

527

## 528 **5. Discussion and Conclusions**

529

530 The main goal of the work presented in this paper is to develop a new wind product capable of  
531 addressing the main limitations of two of the most commonly used methods for generating the  
532 existing wind datasets: satellite data and numerical weather prediction models. For this purpose, wind  
533 data from scatterometers, radiometers, Synthetic-aperture radar and a wind forecasting model are  
534 combined and the potential improvements of the new analyses were assessed by comparison with a  
535 network of offshore buoys moored along the Iberian Peninsula coast. The results show that blended  
536 winds improve the agreement with wind observations, reducing the bias and improving every  
537 statistical score evaluated. The scatter of the satellite wind speed analysis is reduced for almost all  
538 wind speed ranges further reducing the magnitude of the wind power estimation error.

539 Several wind atlases are already publicly available and have been used for site selection and for  
540 designing energy harnessing systems worldwide. These use data mainly from reanalysis datasets or  
541 satellite information. However, these tools can still introduce uncertainty from its main components:  
542 mesoscale and microscale modelling. Similarly, several studies have already provided reasonably  
543 accurate estimates of the wind speed and energy resources in the region that concerns this work by  
544 using numerical models. The main strength of the dataset presented is the fact that since the WRF  
545 model has been used in this area in several studies, the combination of physical parameterizations  
546 used here with satellite data aims at providing better results than the ones we would obtain from the  
547 existing reanalysis and wind maps.

548 The main strength of this research is that it uses the existing knowledge obtained from the multiple  
549 sensitivity and assessment studies in this geographical area in combination with skilful satellite data  
550 to create improved wind information for the Portuguese coast.

551 The second part of this work presents an example of an application of this new wind dataset: an  
552 improved regional wind atlas to identify suitable areas for wind parks.

553 To give an example of the applications of this product a spatial and temporal analysis of the wind  
554 patterns is also carried out. The results show that a significant percentage of the winds vary from 5.5  
555 to 8.5 m/s and despite some seasonal and interannual variations, the conditions are very attractive for  
556 new wind projects. As expected from a location in the northern hemisphere, winter presents a more  
557 energetic season with stronger winds over the entire domain and a higher probability of occurrence  
558 of extreme events.

559 Though locations close to the shoreline are still economically profitable, it is shown that the wind  
560 rapidly increases with the distance to the coast. Analyzing the energy projections, it can be concluded  
561 that northern regions concentrate most of the energy consistently throughout the seasons. Overall, the

562 energy hot spots are located in the central and northern regions with the energy attaining its maximum  
563 at the northwest corner of the Peninsula. Still, the wind power class is above the threshold of three  
564 for all seasons and years which confirms the economic feasibility at this preliminary assessment stage.  
565 At Porto and Ericeira, two promising areas to harness energy in its vicinity, around 350-400 W/m<sup>2</sup>  
566 are available for extraction, on average, during the 2004-2012 period. When comparing the results  
567 against the data from wind atlas, differences up to 200 W/m<sup>2</sup> from the estimated wind power can be  
568 detected, which provides additional support that the choice of the dataset is of utmost importance for  
569 site selection.

570 Looking into the results provided by the newly generated wind maps shows that the entire area is  
571 promising for renewable energies, but a high wind energy site alone is not the only requirement for  
572 building wind parks. The next step would be combining the results of this study with the existing  
573 knowledge on the limitations imposed by physical and environmental constraints such as distance to  
574 shore, biodiversity protection, shipping routes, military areas, human activity, oil and gas exploration  
575 and tourist zones. [58]

576 Finally, the new blended winds can be used to generate time series for promising sites around the  
577 world along with the estimation of the maximum wind energy yield for use in renewable energy  
578 system models. The techniques described in this paper can be applied to any test site and help correct  
579 numerical model bias, improving future wind integration studies.

580

## 581 **5 Acknowledgements**

582

583 This work was conducted within the ARCWIND project—Adaptation and implementation of floating  
584 wind energy conversion technology for the Atlantic region (EAPA 344/2016), which is co-financed  
585 by the European Regional Development Fund through the Interreg Atlantic Area Programme. This  
586 work contributes to the Strategic Research Plan of the Centre for Marine Technology and Ocean  
587 Engineering (CENTEC), which is financed by the Portuguese Foundation for Science and  
588 Technology (Fundação para a Ciência e Tecnologia - FCT) under contract UIDB/UIDP/00134/2020.

589

590

## 591 **References**

592 [1] Palin, E.J., Scaife, A.A., Wallace, E., Pope, E.C.D., Arribas, A. and Brookshaw, A. (2016). Skillful  
593 Seasonal Forecasts of Winter Disruption to the U.K. Transport System. *Journal of Applied*  
594 *Meteorology and Climatology*, 55(2), 325–344.

- 595 [2] Bett, P.E., Thornton, H.E., Lockwood, J.F., Scaife, A.A., Golding, N., Hewitt, C., Zhu, R., Zhang,  
596 P.Q. and Li, C.F. (2017). Skill and Reliability of Seasonal Forecasts for the Chinese Energy Sector.  
597 *Journal of Applied Meteorology and Climatology*, 56(11), 3099–3114.
- 598 [3] Diaz, H.M. and Guedes Soares, C. (2020) Review of the current status, technology and future  
599 trends of offshore wind farms. *Ocean Engineering*. 209:107381
- 600 [4] Castro-Santos, L., Martins, E. and Guedes Soares, C. (2016) Cost assessment methodology for  
601 combined wind and wave floating offshore renewable energy systems. *Renewable Energy*. 97:866-  
602 880.
- 603 [5] Castro-Santos, L., Silva, D., Bento, A.R., Salvação, N. and Guedes Soares, C. (2020) Economic  
604 feasibility of floating offshore wind farms in Portugal. *Ocean Engineering*. 207:107393
- 605 [6] Castro-Santos, L., Bento, A.R., Silva, D., Salvação, N. and Guedes Soares, C. (2020) Economic  
606 feasibility of floating offshore wind farms in the north of Spain. *Journal of Marine Science and*  
607 *Engineering*. 8(1):58-76.
- 608 [7] Christoforaki, M. and Tsoutsos, T. (2017), “Sustainable siting of an offshore wind park a case in  
609 Chania, Crete”, *Renewable Energy*, Vol. 109, pp. 624-633.
- 610 [8] Diaz, H.M. and Guedes Soares, C. (2020); An integrated GIS approach for site selection of floating  
611 offshore wind farms in the Atlantic Continental European coastline. *Renewable and Sustainable*  
612 *Energy Reviews*. 134:110328
- 613 [9] Diaz, H.M., Fonseca, R.B. and Guedes Soares, C. (2019) Site selection process for floating  
614 offshore wind farms in Madeira Islands. Guedes Soares, C., (Eds.). *Advances in Renewable Energies*  
615 *Offshore*. Taylor & Francis; pp. 729-737.
- 616 [10] Diaz, H.M. and Guedes Soares, C. (2021) A multi-criteria approach to evaluate floating offshore  
617 wind farms siting in the Canary Islands (Spain). *Energies*. 14:865
- 618 [11] Goodess, C.M., Troccoli, A., Acton, C., Añel, J.A., Bett, P.E., Brayshaw, D.J., De Felice, M.,  
619 Dorling, S.R., Dubus, L., Penny, L., Percy, B., Ranchin, T., Thomas, C., Trolliet, M., Wald, L. (2019)  
620 *Advancing climate services for the European renewable energy sector through capacity building and*  
621 *user engagement*, *Climate Services*, 16,2019,100139,ISSN 2405-8807
- 622 [12] Dee, D.P., Uppala, S.M., Simmons, A.J., Berrisford, P., Poli, P., Kobayashi, S., Andrae, U.,  
623 Balsameda, M.A., Balsamo, G., Bauer, P., Bechtold, P., Beljaars, A.C.M., Van de Berg, L., Bidlot, J.,  
624 Bormann, N., Delsol, C., Dragani, R., Fuentes, M., Geer, A. J., Haimberger, L., Healy, S.B., Hersbach,  
625 H., Hólm, E.V., Isaksen, I., Kållberg, P., Köhler, M., Matricardi, M., McNally, A. P., Monge-Sanz,  
626 B. M., Morcrette, J.-J., Park, B.-K., Peubey, C., Rosnay, P., Tavolato, C., Thépaut and F. Vitart, J.-N.,  
627 2011. The ERA-Interim reanalysis: Configuration and performance of the data assimilation system.  
628 *Quart. J. R. Meteorol. Soc.*, 137, 553-597.

- 629 [13] Copernicus Climate Change Service ERA5 monthly averaged data on single levels from 1979 to  
630 present ECMWF (2019)
- 631 [14] Gelaro, R., McCarty, W., Suárez, M.J., Todling, R., Molod, A., Takacs, L., Randles, C.A.,  
632 Darmenov, A., Bosilovich, M.G., Reichle, R., Wargan, K., Coy, L., Cullather, R., Draper, C., Akella,  
633 S., Buchard, V., Conaty, A., da Silva, A.M., Gu, W., Kim, G.-K., Koster, R., Lucchesi, R., Merkova,  
634 D., Nielsen, J.E., Partyka, G., Pawson, S., Putman, W., Rienecker, M., Schubert, S.D., Sienkiewicz,  
635 M., Zhao, B. (2017) The modern-era retrospective analysis for research and applications, version 2  
636 (MERRA-2) *J Clim*, 30 (14), pp. 5419-5454
- 637 [15] González-Aparicio, I., Monforti, F., Volker, P., Zucker, A., Careri, F., Huld, T. and Badger, J.  
638 (2017). Simulating European wind power generation applying statistical downscaling to reanalysis  
639 data, *Applied Energy*, Volume 199, Pages 155-168.
- 640 [16] Gruber, K., Regner, P., Wehrle, S., Zeyringer, M. and Schmidt, J. (2022). Towards global  
641 validation of wind power simulations: A multi-country assessment of wind power simulation from  
642 MERRA-2 and ERA-5 reanalysis bias-corrected with the global wind atlas, *Energy*, Volume 238, Part  
643 A, 121520.
- 644 [17] Al-Yahyai, S., Charabi, Y. and Gastli, A. (2010). Review of the use of Numerical Weather  
645 Prediction (NWP) Models for wind energy assessment. *Renewable and Sustainable Energy Reviews*,  
646 14(9), 3192–3198.
- 647 [18] Salvação, N. and Guedes Soares, C. (2016) Resource assessment methods in the offshore wind  
648 energy sector. L. Castro-Santos and V. Diaz-Casas (Eds.). *Floating Offshore Wind Farms*. Springer  
649 International Publishing Switzerland; pp. 121-141.
- 650 [19] Salvação, N., Bernardino, M. and Guedes Soares, C., 2014. Assessing mesoscale wind  
651 simulations in different environments. *Computers & Geosciences*, Volume 71, October 2014, Pages  
652 28-36.
- 653 [20] Jesus, F.D., Menéndez, M., Guanche, R. and Losada, I. (2014). A wind chart to characterize  
654 potential offshore wind energy sites. *Computers & Geosciences*, 71, 62–72.
- 655 [21] Charabi, Y., Al-Yahyai, S. and Gastli, A. (2011). Evaluation of NWP performance for wind  
656 energy resource assessment in Oman. *Renewable and Sustainable Energy Reviews*, 15(3), 1545–  
657 1555.
- 658 [22] Karagali, I., Badger, M. Hahmann, A.N., Peña, A. Hasaber, C.B. and Sempreviva, A.M. (2013),  
659 “Spatial and temporal variability of winds in the Northern European Seas”, *Renewable Energy*, Vol.  
660 57, pp. 200-210.
- 661 [23] Nawri, N., Petersen, G.N., Bjornsson, H., Hahmann, A.N., Jónasson, K., Hasager, C.B. and  
662 Clausen, N-E. (2014), “The wind energy potential of Iceland”, *Renewable Energy*, Vol. 69, pp. 290-  
663 299.

- 664 [24] Salvação, N. and Guedes Soares C., (2018). Wind resource assessment offshore the Atlantic  
665 Iberian coast with the WRF model. *Energy*, 145, 276–287.
- 666 [25] Al-Yahyai, S., Charabi, Y., Al-Badi, A. and Gastli, A. (2012), “Nested ensemble NWP approach  
667 for wind energy assessment”, *Renewable Energy*, Vol. 37, pp. 150-160.
- 668 [26] Mylonas, M.P., Barbouchi, S., Herrmann, H. and Nastos, P.T. (2018), “Sensitivity analysis of  
669 observational nudging methodology to reduce error in wind resource assessment (WRA) in the North  
670 Sea”, *Renewable Energy*, Vol. 120, pp. 446-456.
- 671 [27] Linaje, N.G.-A., Mattar, C. and Borvarán, D. (2019). Quantifying the wind energy potential  
672 differences using different WRF initial conditions on Mediterranean coast of Chile. *Energy*, 188,  
673 116027.
- 674 [28] Zhao, J., Guo, Y., Xiao, X., Wang, J., Chi, D. and Guo, Z. (2017). Multi-step wind speed and  
675 power forecasts based on a WRF simulation and an optimized association method. *Applied Energy*,  
676 197, 183–202.
- 677 [29] Naidu, N., Nagababu, G., Kachhwaha, S. and Savsani, V. (2016). Evaluation of offshore wind  
678 power potential of India by combining satellite and moored buoy data. Guedes Soares, C., (Ed.),  
679 *Progress in Renewable Energies Offshore*. London, UK: Taylor & Francis Group, pp. 153-158.
- 680 [30] Kumar, S.V.A., Nagababu, G. and Kumar, R. (2019). Comparative study of offshore winds and  
681 wind energy production derived from multiple scatterometers and met buoys. *Energy*, 185, 599–611.
- 682 [31] Guo, Q., Huang, R., Zhuang, L., Zhang, K. and Huang, J. (2019). Assessment of China’s  
683 Offshore Wind Resources Based on the Integration of Multiple Satellite Data and Meteorological  
684 Data. *Remote Sensing*, 11(22), 2680.
- 685 [32] Chang, R., Zhu, R., Badger, M., Hasager, C., Xing, X. and Jiang, Y. (2015). Offshore Wind  
686 Resources Assessment from Multiple Satellite Data and WRF Modeling over South China Sea.  
687 *Remote Sensing*, 7(1), 467–487.
- 688 [33] Hasager, C.B., Hahmann, A.N., Ahsbahs, T., Karagali, I., Sile, T., Badger, M. and Mann, J.  
689 (2019). Europe’s offshore winds assessed from SAR, ASCAT and WRF., *Wind Energy Science*  
690 <https://doi.org/10.5194/wes-2019-38>
- 691 [34] Guo, Q., Xu, X., Zhang, K., Li, Z., Huang, W., Mansaray, L. and Huang, J. (2018). Assessing  
692 Global Ocean Wind Energy Resources Using Multiple Satellite Data. *Remote Sensing*, 10(2), 100.
- 693 [35] Nezhad, M.M., Groppi, D., Marzialetti, P., Fusilli, L., Laneve, G., Cumo, F. and Garcia, D.A.  
694 (2019). Wind energy potential analysis using Sentinel-1 satellite: A review and a case study on  
695 Mediterranean islands. *Renewable and Sustainable Energy Reviews*, 109, 499–513.
- 696 [36] Carvalho, D., Rocha, A., Gómez-Gesteira, M. and Santos, C.S. (2017). Offshore winds and wind  
697 energy production estimates derived from ASCAT, OSCAT, numerical weather prediction models and

- 698 buoys – A comparative study for the Iberian Peninsula Atlantic coast. *Renewable Energy*, 102, 433–  
699 444.
- 700 [37] Carvalho, D., Rocha, A., Gómez-Gesteira, M., Alvarez, I. and Santos, C.S. (2013). Comparison  
701 between CCMP, QuikSCAT and buoy winds along the Iberian Peninsula coast. *Remote Sensing of*  
702 *Environment*, 137, 173–183.
- 703 [38] Santos, F.; Gómez-Gesteira, M.; deCastro, M.; Añel, J.A.; Carvalho, D.; Dias, J.M. (2018). On  
704 the accuracy of CORDEX RCMs to project future winds over the Iberian Peninsula and surrounding  
705 ocean. *Applied Energy*, 228(), 289–300. doi:10.1016/j.apenergy.2018.06.086
- 706 [39] Campos, R.M. and Guedes Soares, C. (2018). Spatial distribution of offshore wind statistics on  
707 the coast of Portugal using Regional Frequency Analysis. *Renewable Energy*. 123:806-816.
- 708 [40] Wang, J., Qin, S., Jin, S. and Wu, J. (2015). Estimation methods review and analysis of offshore  
709 extreme wind speeds and wind energy resources. *Renewable and Sustainable Energy Reviews*, 42,  
710 26–42.
- 711 [41] [www.emodnet.eu](http://www.emodnet.eu)
- 712 [42] Fairall, C.W., Bradley, E.F., Hare, J.E., Grachev, A.A. and Edson, J.B. (2003). Bulk  
713 Parameterization of Air–Sea Fluxes: Updates and Verification for the COARE Algorithm. *Journal of*  
714 *Climate*, 16(4), 571–591
- 715 [43] Wang, W., Barker, D., Bray, J., Bruyere, C., Duda, M. and Dudhia, J. User's guide for advanced  
716 research WRF (ARW) modeling system version 3. Mesoscale and microscale meteorology division.  
717 National Center for Atmospheric Research (MMM-NCAR); 2007.
- 718 [44] Bentamy, A., Mouche, A., Grouazel, A., Moujane, A. and Mohamed, A.A. (2018). Using  
719 sentinel-1A SAR wind retrievals for enhancing scatterometer and radiometer regional wind analyses.  
720 *International Journal of Remote Sensing*, 40(3), 1120–1147.
- 721 [45] Desbiolles, F., Bentamy, A., Blanke, B., Roy, C., Mestas-Nuñez, A.M., Grodsky, S.A., Herbette,  
722 S., Cambon, G. and Maes, C. (2017). Two decades [1992–2012] of surface wind analyses based on  
723 satellite scatterometer observations. *Journal of Marine Systems*, 168, 38–56.
- 724 [46] Wentz, F.J. (2013). SSM/I Version-7 Calibration Report, report number 011012, Remote Sensing  
725 Systems, Santa Rosa, CA, 46pp.
- 726 [47] Bentamy, A., Croize-Fillon, D. and Perigaud, C. (2008). Characterization of ASCAT  
727 measurements based on buoy and QuikSCAT wind vector observations. *Ocean Science*, 4(4), 265–  
728 274.
- 729 [48] Gómez, G., Cabos, W.D., Liguori, G., Sein, D., Lozano-Galeana, S., Fita, L., Fernández, J.,  
730 Magariño, M.E., Jimenez-Guerrero, P., Montávez, J.P., Dominguez, M., Romera, R. and Gaertner, M.  
731 (2015). Characterization of the wind speed variability and future change in the Iberian Peninsula and  
732 the Balearic Islands. *Wind Energy*, 19(7), 1223–1237.

- 733 [49] Patlakas, P., Galanis, G., Barranger, N. and Kallos, G. (2016). Extreme wind events in a complex  
734 maritime environment: Ways of quantification. *Journal of Wind Engineering and Industrial*  
735 *Aerodynamics*, 149, 89–101
- 736 [50] Hahmann, A. N., Sīle, T., Witha, B., Davis, N. N., Dörenkämper, M., Ezber, Y., García-  
737 Bustamante, E., González-Rouco, J. F., Navarro, J., Olsen, B. T., & Söderberg, S. (2020). The making  
738 of the New European Wind Atlas – Part 1: Model sensitivity. *Geoscientific Model Development*,  
739 13(10), 5053-5078.
- 740 [51] Bailey, H. & Brookes, K. and Thompson, P. (2014). Assessing Environmental Impacts of  
741 Offshore Wind Farms: Lessons Learned and Recommendations for the Future. *Aquatic biosystems*.  
742 10. 8. 10.1186/2046-9063-10-8
- 743 [52] Al-Hinai, A.; Charabi, Y.; Aghay Kaboli, S.H. Offshore Wind Energy Resource Assessment  
744 across the Territory of Oman: A Spatial-Temporal Data Analysis. *Sustainability* 2021, 13, 2862
- 745 [53] Dupont, E., Koppelaar, R. and Jeanmart, H. (2017). Global available wind energy with physical  
746 and energy return on investment constraints. *Applied Energy*. 209. 10.1016/j.apenergy.2017.09.085.
- 747 [54] Jerez, S., Trigo, R. M., Vicente-Serrano, S. M., Pozo-Vázquez, D., Lorente-Plazas, R., Lorenzo-  
748 Lacruz, J., Santos-Alamillos, F., & Montávez, J. P. (2013). The Impact of the North Atlantic  
749 Oscillation on Renewable Energy Resources in Southwestern Europe, *Journal of Applied*  
750 *Meteorology and Climatology*, 52(10), 2204-2225
- 751 [55] Soares P. M. M., Cardoso R. M., Semedo A., Chinita M.J. and Ranjha R. (2014) Climatology of  
752 the Iberia coastal low-level wind jet: weather research forecasting model high-resolution results,  
753 *Tellus A: Dynamic Meteorology and Oceanography*, 66:1, 22377
- 754 [56] Oh, K.-Y., Kim, J.-Y., Lee, J.-S. and Ryu, K.-W. (2012). Wind resource assessment around  
755 Korean Peninsula for feasibility study on 100 MW class offshore wind farm. *Renewable Energy*, 42,  
756 217–226.
- 757 [57] Salvação, N., Guedes Soares, C. and Bentamy, A. (2019), Estimating the offshore wind energy  
758 along the Portuguese coast using WRF and satellite data”, *Advances in Renewable Energies Offshore*,  
759 Guedes Soares, C. (Ed.), Taylor & Francis Group, London, UK, pp. 703-710
- 760 [58] Salvador S., Gimeno L., Javier Sanz Larruga F., (2019) The influence of maritime spatial  
761 planning on the development of marine renewable energies in Portugal and Spain: Legal challenges  
762 and opportunities, *Energy Policy*, Volume 128, Pages 316-328, ISSN 0301-4215.

**Declaration of interests**

- The authors declare that they have no known competing financial interests or personal relationships that could have appeared to influence the work reported in this paper.
- The authors declare the following financial interests/personal relationships which may be considered as potential competing interests:

Journal Pre-proof